The rate of substitution from η ^{6}-arene ruthenium(II) complexes

Meshack K. Sitati, Deogratius Jaganyi & Allen Mambanda

Springer

Springer

The rate of substitution from η^6-arene ruthenium(II) complexes

Meshack K. Sitati[1] · Deogratius Jaganyi[2,3] · Allen Mambanda[1]

Abstract

The rate and mechanism of substitution in the Ru(II) complexes (C1–C6) by thiourea nucleophiles was studied at pH 2 and rate constants measured as a function of nucleophile concentrations and temperature using spectrometric methods. There is increased electron density at the Ru metal atom of C2 as a result of inductive donation by substituents on the arene ligand, making it less positive and therefore less reactive than C1. For the complexes C3–C6 bearing the 2,2′-bipyridyl ligand, the aqua ligands are located trans to the arene ligands, and hence, their reactivity increases in accordance to the number and type of alkyl substituents on the η^6-arene ligands which donate inductively into the π-molecular orbitals, causing increased trans labialisation of the coordinated aquo co-ligand. Compared to the reactivity of triaquo complex (C1), the auxiliary bipyridyl ligand of (C3) complex lowers the rate of substitution for the later complex by a factor of about 100, possibly due to its steric hindrance at the Ru(II) metal centre. The significantly negative activation entropies and positive activation enthalpies suggest an associative mode of substitution. The reactivity of the nucleophiles follow the order DMTU > TU > TMTU.

Introduction

Interaction of transition metal complexes with DNA is one of the major known mechanistic pathways responsible for the anti-tumour activity [1–5]. Through such molecular mechanism of interaction, the prototype anti-cancer drug, cisplatin is active against several human cancer cell lines including those of the pancreatic, head, neck and testicular [6, 7]. However, it is acutely toxic to the kidneys and ineffective against several other cancers as well as being prone to development of resistance.

✉ Deogratius Jaganyi
deojaganyi@gmail.com

Meshack K. Sitati
meshacksitati@gmail.com

1 School of Chemistry and Physics, University of KwaZulu-Natal, Private Bag X01, Scottsville, Pietermaritzburg 3209, South Africa

2 School of Science, College of Science and Technology, University of Rwanda, P.O. Box 4285, Kigali, Rwanda

3 Department of Chemistry, Faculty of Applied Sciences, Durban University of Technology, P.O. Box 1334, Durban 4000, South Africa

An attractive class of complexes that can be an alternative to Pt-based cancer drugs is ruthenium (Ru) complexes. Ru complexes are significantly less toxic because they can role-play iron binding modes in biological systems [8–12]. Leading Ru complexes which have been evaluated in vitro and in vivo [13] for cytotoxicity and showed promising activity profiles include imidazolium-trans-[tetrachloro(dimethyl sulfoxide)imidazole-ruthenium(III)] (NAMI-A) and indazolium trans-[tetrachlorobis(1H-indazole)-ruthenium(III)] (KP 1019). They have also shown great anti-cancer potential in clinical trials [14].

A subclass of Ru complexes that has been extensively evaluated for the anti-cancer activity are arene Ru(II) complexes. Examples include $[(\eta^6\text{-biphenyl})\text{Ru(en)Cl}]^+$ (en = ethylenediamine) [9] and $[(\eta^6\text{-p-cymene})\text{Ru(PTA)Cl}_2]$ (PTA = 1,3,5-triaza-7-phosphaadamantane) [15–17]. These too have shown great potential as anti-cancer agents [6, 18–21]. Numerous studies have linked their superior anti-cancer activity to the extra and favourable non-covalent interactions between the arene ligands on the Ru complexes with hydrophobic components of cell membranes and at the ultimate nucleophilic target, DNA [22–25]. Cytotoxicity of the arene-Ru complexes has been positively correlated to the nature of the substituents on the arene as well as other rings conjugated to it. The hydrophobic face within the backbone of the non-leaving ligand of the complexes enhances bimolecular recognition on the non-polar receptor sites of

the target macro-nucleophiles [22, 26–28]. Substitution of the labile halogen ligands by a chelating ligand can help to control the stability and ligand exchange kinetics of these complexes [29–31]. Previous studies have focused more on DNA binding and cytotoxicity studies leaving a gap on the kinetic properties of the complexes. Recognizing the importance of the kinetics and mechanism of the interaction of metal-based drugs with DNA, this work investigated the rate of substitution from benzene(triaquo)ruthenium(II)perchlorate, C1, mesitylene(triaquo)ruthenium(II)perchlorate, C2, aquo(benzene)-2,2′-bipyridineruthenium(II)perchlorate, C3, aquo-2,2′-bipyridine-(mesitylene)ruthenium(II)perchlorate, C4, aqua-2,2′-bipyridine(hexamethylbenzene)-ruthenium(II) perchlorate, C5 and aqua-2,2′-bipyridine(p-cymene) ruthenium(II)perchlorate, C6 by thiourea nucleophiles viz. thiourea(TU), 1,3-dimethyl-2-thiourea(DMTU) and 1,1,3,3-tetramethyl-2-thiourea (TMTU). The study seeks to establish the role of arene ligands on the rate of substitution from these complexes. The chemical structures of the complexes used in this study are shown in Fig. 1.

Experimental

Materials and synthesis

All chemicals including ligands, the dichloro(arene)Ru(II) dimers, solvents, silver perchlorate and perchloric acid were purchased from Sigma-Aldrich and used as received. The complexes 2,2′-bipyridine(p-cymene)ruthenium(II) dichloride, benzene-2,2′-bipyridineruthenium(II) dichloride, 2,2′-bipyridine(mesitylene)ruthenium(II) dichloride and 2,2′-bipyridine(hexamethylbenzene)ruthenium(II) dichloride were synthesized according to published procedures [32] as
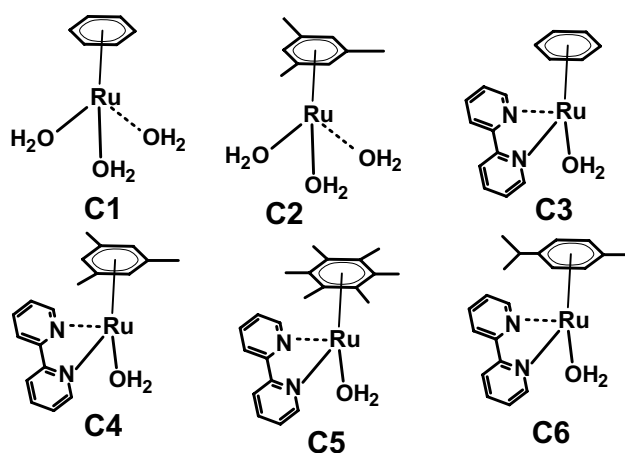

Fig. 1 Chemical structures of η^6-arene Ru(II) complexes [the charges (2+) and counter ions (Cl−) have been left out for clarity]

follows. (The atomic numbering applied on C1–C6 for the presentation of their calculated data as well as the discussion of the influence of their non-leaving ligands on the rate of substitution is illustrated here by Fig. 2 for C3.)

Preparation of 3,2′-bipyridine(p-cymene) ruthenium(II) dichloride

Dichloro(p-cymene)ruthenium(II) dimer (91.86 mg, 0.15 mmol) was added to a solution of 2,2′-bipyridine (46.85 mg, 0.3 mmol) in ethanol (15 mL) and the reaction mixture heated at reflux for 6 h. The resulting solution was cooled to room temperature and the precipitate of the complex obtained by addition of diethyl ether (60 mL). The precipitate was filtered off, washed with diethyl ether and pentane then dried in air. Yield: 127.62 mg (92%). ^{1}H NMR (400 MHz, CD$_3$OH) δ/ppm, J/Hz: 9.49 (d, 2H, 1, 1′, $J = 5.5$); 8.51 (d, 2H, 4 4′, $J = 8.2$); 8.25 (t, 2H, 3, 3′, $J = 15.8$); 7.78 (dd, 2H, 2, 2′, $J = 5.6$, $J = 2.0$); 6.12 (d, 2H, –CH$_2$, $J = 6.2$); 5.86 (d, 2H, –CH$_2$, $J = 6.5$); 2.64 (m, 1H, CH); 2.28 (S, 3H, –CH$_3$); 1.05 (d, 6H, –CH$_3$, $J = 6.2$). ^{13}C NMR (75 MHz,
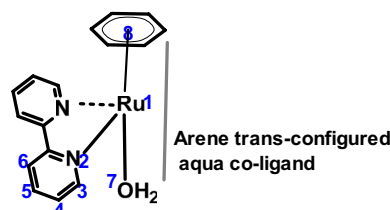

Fig. 2 An illustration of the numbering using C3 as an example

MeOH), δ/ppm: 17.55, 20.87, 30.96, 84.14, 86.82, 104.44, 104.65, 123.57, 127.49, 139.79, 154.98, 155.48. Anal. Calcd. for C$_{20}$H$_{22}$Cl$_2$N$_2$Ru: C, 51.95; H, 4.80; N, 6.06; Found: C, 51.85; H, 5.01; N, 6.26. ESI$^+$ LCMS, m/z: 426 [M]$^+$.

Preparation of benzene-2,2′-bipyridineruthenium (II) dichloride

The compound was synthesised following the same procedure as that of 2,2′-bipyridine(p-cymene)ruthenium(II) dichloride using 2,2′-bipyridine (46.85 mg, 0.3 mmol) and benzeneruthenium(II) chloride dimer (75.02 mg, 0.15 mmol). Yield: 97.50 mg (80%). ^{1}H NMR (400 MHz, CD$_3$OH) δ/ppm, J/Hz: 9.60 (d, 2H, 1, 1′, $J = 5.4$); 8.53 (d, 2H, 4,4′, $J = 7.9$); 8.26 (t, 2H, 3,3′, $J = 15.8$); 7.77 (dd, 2H, 2 2′, $J = 5.7$, $J = 2.3$); 6.12 (s, 6H, –CH$_3$). ^{13}C NMR (75 MHz, MeOH), δ/ppm: 88.64, 125.03, 128.77, 141.28, 156.62, 157.07. Anal. Calcd. for C$_{16}$H$_{14}$Cl$_2$N$_2$Ru: C, 47.30; H, 3.47;

N, 6.90; Found: C, 47.18; H, 3.71; N, 6.88. ESI$^+$ LCMS, m/z: 371 [M]$^+$.

Preparation of 2,2′-bipyridine(mesitylene) ruthenium(II) dichloride

The compound was prepared following the same procedure as that of 2,2′-bipyridine(p-cymene)ruthenium(II) dichloride using 2,2′-bipyridine (46.85 mg, 0.3 mmol) and benzeneruthenium(II) chloride dimer (87.65 mg, 0.15 mmol). Yield: 93.48 mg (70%). ^{1}H NMR (400 MHz, CD$_3$OH) δ/ppm, J/Hz: 9.30 (d, 2H, 1,1′, $J = 5.9$); 8.44 (d, 2H, 4 4′, $J = 8.2$); 8.17 (t, 2H, 3 3′, $J = 15.8$); 7.73 (dd, 2H,2 2′, $J = 5.6$, $J = 2.0$); 5.48 (s, 3H, –CH); 2.16 (s, 9H, –CH$_3$). ^{13}C NMR (75 MHz, MeOH), δ/ppm: 17.40, 79.40, 107.42, 123.03, 127.45, 139.63, 154.82, 155.35. Anal. Calcd for C$_{19}$H$_{20}$Cl$_2$N$_2$Ru: C, 50.90; H, 4.50; N, 6.25; Found: C, 50.51; H, 4.54; N, 6.45. ESI$^+$ LCMS, m/z: 413 [M]$^+$.

Preparation of 2,2′-bipyridine(hexamethylbenzene) ruthenium(II) dichloride

The following compound was prepared following the same procedure as that of 2,2′-bipyridine(p-cymene)ruthenium(II) dichloride using 2,2′-bipyridine (46.85 mg, 0.3 mmol) and dichloro(hexamethylbenzene)ruthenium(II) dimer (100.27 mg, 0.15 mmol). Yield: 118.62 mg (83%). ^{1}H NMR (400 MHz, CD$_3$OH) δ/ppm, J/Hz: 8.87 (d, 2H, 1,1′, $J = 5.7$); 8.37 (d, 2H, 4,4′, $J = 8.2$); 8.10 (t, 2H, 3,3′, $J = 15.8$); 7.69 (dd, 2H,2,2′, $J = 5.4$, $J = 1.2$); 2.02 (s, 18H, –CH$_3$). ^{13}C NMR (75 MHz, MeOH), δ/ppm: 15.67, 97.39, 124.63, 128.91, 140.91, 155.05, 156. Anal. Calcd for C$_{22}$H$_{26}$Cl$_2$N$_2$Ru, %: C, 53.88; H, 5.34; N, 5.71; Found: C: 54.19; H: 5.42; N: 5.34. ESI$^+$ LCMS, m/z: 455 [M]$^+$.

The synthesized compounds were characterized by elemental analysis and spectroscopic techniques, giving satisfactory data. They are stable in air as solids or their solutions. All compounds gave ^{1}H and ^{13}C NMR spectra corresponding to the proposed formulations. Mass spectrometric data gave isotopic pattern distribution corresponding to the nominal masses of the complexes without the counter ions. The elemental analysis data were in agreement to the theoretical CHN values to within ± 0.40. The sample spectra for NMR and mass analyses are placed in the supporting information Fig. ESI1–12.

## Preparation of aqua Ru(II) complexes (C1–6)

The desired solutions of the aqua complexes for kinetic studies were prepared from the chloride derivatives according to a literature procedure [33]. To a stirred solution of the chloro complexes in 0.01 M perchloric acid (HClO$_4$) (40 mL) was added silver perchlorate (AgClO$_4$). The moles of silver chloride added were slightly lower (< 0.1%) equivalent to the number of chloride ions in the complex. The mixture was stirred for 24 h at 50 °C in the dark, cooled and filtered using a 0.45 μm nylon membrane filter (Millipore) to remove the precipitated silver chloride. The filtrate was made up to 100 mL using 0.1 M HClO$_4$ which had an ionic strength of 0.1 M adjusted by dissolving 0.09 M NaClO$_4$ in 0.01 M perchloric acid. Kinetic analyses were done at pH 2 for all complexes as the pH titration showed that only aqua species of the complexes exist at this pH [34].

Determination of pK_a of Aqua complexes (C1–6)

The acidities of the aqua ligands were determined before kinetic analysis could be done. The pK_a titrations were done spectrometrically as described in the literature [35–37]. The pH titrations were started with solution of the aqua complexes at pH 2 (0.01 M HClO$_4$ solution) by addition of small amounts of NaOH until pH 9. To avoid errors due to dilution effect, a large volume (300 mL) of complex solution was used. Solid NaOH granules were used in the pH range of 1–3 solutions followed by dropwise addition of 0.5 M or 0.1 M or 0.05 M or 0.001 M of NaOH solution to adjust pH. After each addition of NaOH or acid, the solution was briefly stirred before recording the pH value. Vials were used to sample the solution (~ 2 mL) for pH measurements, and then, the solution was discarded to avoid in situ precipitation of the chloride. The aliquots from spectral acquisitions were returned to the titration solution. Both NaOH and perchloric acid were used to observe the reversibility of the spectra as proof of existence of the deprotonation of the aqua as defined by K_a [34]. The absorbance data were plotted against pH giving a sigmoid curve from which the pK_a values were determined by locating the inflection points. Figure 3 shows a typical UV–visible spectrum recorded during spectrophotometric titration of the aqua complex solutions with NaOH and inset is the sigmoid curve.

The pK_a values in Table 1 indicate that the higher the alkylation of the arene moieties the lower the acidity. This shows a correlation between pK_a values and the electrophilicity of the Ru metal centres. The values/acidity increase in the order: C5~C6~C4~C3 < C1~C2 which is consistent with the electrophilicity of the metal centres. More electrophilic metal centres (of C1 and C2) as supported by DFT NBO calculations have lower pK_a values. The pK_a titration reactions of the aqua complexes with OH$^-$ are illustrated in Scheme 1

$$\left[X\text{-(Bip)-Ru-OH}_2\right]^{n+} + OH^- \overset{K_a}{\rightleftharpoons} \left[X\text{-(Bip)-Ru-OH}\right]^{(n-1)+} + H_2O$$
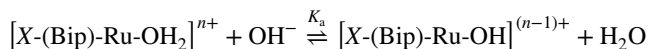
X = benzene or mesitylene or hexamethylbenzene or p-cymene.
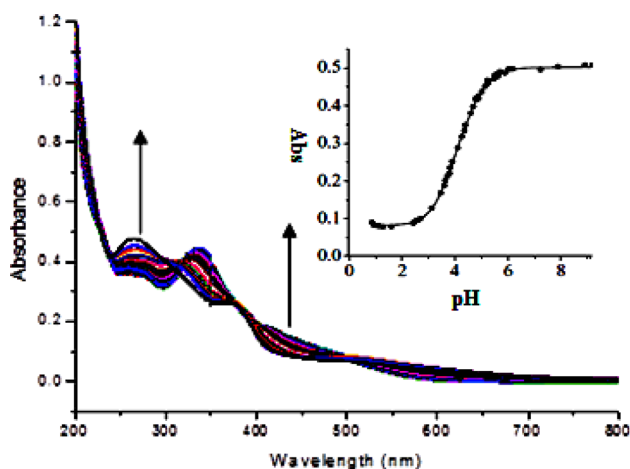
Fig. 3 UV–visible spectra of C1 complex recorded as a function of pH in the range of 2–9 at 25 °C. Inset is a plot of absorbance versus pH at $\lambda = 275$ nm

**Table 1** pK_a values for the deprotonation of the aqua Ru(II) complexes

Complex	pK_a
C1	4.60 ± 0.01
C2	4.31 ± 0.02
C3	6.92 ± 0.01
C4	7.01 ± 0.02
C5	7.34 ± 0.01
C6	7.21 ± 0.01

Instrumentation

Physical measurements

NMR spectroscopy were recorded on a Bruker Avance DPX 400 MHz spectrophotometer at 303 K, and all chemical shift were referenced to those of $(CH_3)_4$. Low resolution electron spray ionization (ESI^+) mass spectra were recorded on the Waters Micromass LCT Premier Spectrometer or Shimadzu LCMS 2020. Elementary analyses were done on a ThermoScientific Flash 2000 elemental analyser. Kinetic measurements for fast reactions were performed on an Applied Photophysics SX20 stopped-flow instrument coupled with an online data acquisition system whose temperature is controlled to within ± 0.1 °C. The slow reactions were monitored using Varian Cary 100 Bio UV–visible spectrophotometer with an attached Varian Peltier temperature controller
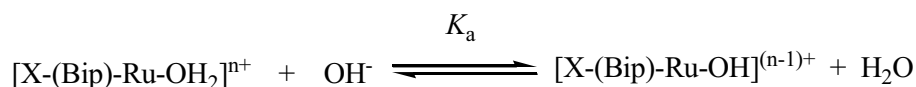
and online kinetic application. The same instrument was used for spectrometric titration. The UV–visible spectrophotometer was also used to predetermine the wavelengths at which the reactions on the stopped-flow were monitored.

Computational modeling

The computations were done by density functional theory (DFT) run on Gaussian 09 suite of programs [38]. The structures were optimized using the hybrid Becke, 3-parameter, Lee–Young–Parr (B3LYP) method with LANL2DZ (Los Alamos National Laboratory 2 double ζ) basis sets having inner core electrons of the Ru atom replaced by relativistic effective core potential (ECP) [39–41]. DFT applies to physically observable electron density over a wave function in the determination of the properties of a system. Los Alamos National Laboratory 2 double ζ basis set exploits relativistic effective core potentials to account for effect of inner core 28 electrons $([Ar]3d^{10})$ in Ru [42, 43]. To take into account of the solvent effects, the complexes were fully optimized in methanol using the conductor polarizable continuum model (C-PCM) [44, 45]. The singlet states were used due to the low electronic spin state of Ru(II) complexes. The complexes were considered to have an overall charge of $+2$. The chemical potential (μ) and molecular hardness (η) for each structure were calculated from the HOMO and LUMO energies. The global electrophilicities (ω) were determined by the relationship $\omega = \mu^2/2\eta$ [46, 47]. The charge on each atom is expressed as a natural bond orbitals (NBO) [48].
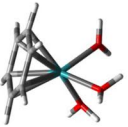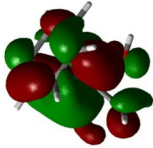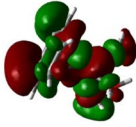
Computational results
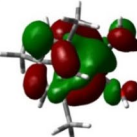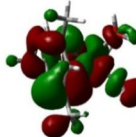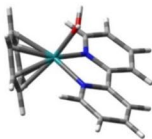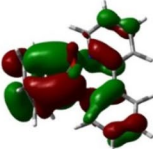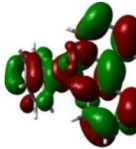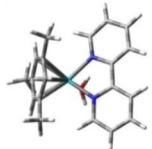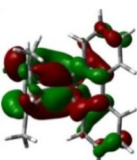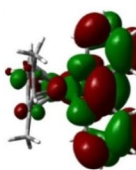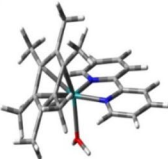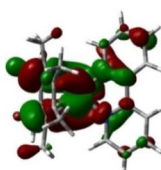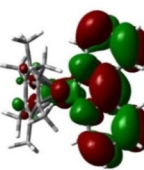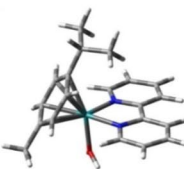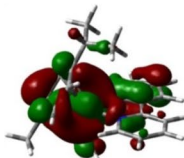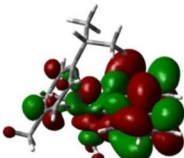
Density functional theory (DFT) [49, 50] calculated data, for example electrophilicity index and NBO charges have provided information in support of the trends observed in the chemical reactivity of the complexes. In this context, several reactivity descriptors have been proposed and used to analyse chemical reactivity and site selectivity. Hardness, η, electronic chemical potential, μ, electrophilicity, ω, are among the reactivity descriptors widely used to understand the global nature of molecules in terms of their stability and it is possible to gain knowledge about the reactivity of molecules. Atomic charges (NBO) are among the local reactivity descriptors, which provide information about the site selectivity [51, 52].

Scheme 1 The titration reactions of the aqua complexes with OH⁻

$$[X\text{-}(Bip)\text{-}Ru\text{-}OH_2]^{n+} \; + \; OH^- \; \underset{\xrightarrow{\hspace{1.5cm}}}{\overset{K_a}{\rightleftharpoons}} \; [X\text{-}(Bip)\text{-}Ru\text{-}OH]^{(n-1)+} \; + \; H_2O$$

X = Benzene or mesitylene or hexamethylbenzene or p-cymene

In this study, computational calculations and optimization were carried out to gain information on the electronic and structural properties of the complexes. The DFT-optimized structures of the complexes are shown in Table 1, and a summary of selected DFT data are presented in Table 2. Examining DFT diagrams in Table 1, the HOMO are located mainly on the ruthenium metal centre and partially on the arene and aqua ligands while the LUMO is entirely on the bipyridine ligand as reported in the literature for other similar studies [53].

Kinetic analysis and results

The rate of substitution of the aqua ligands from the complexes was carried out under pseudo-first-order conditions using at least a tenfold excess of the entering nucleophile for complexes C3, C4, C5 and C6 and at least 30-fold excess for C1 and C2. The kinetics of substituting the aqua ligands was investigated spectrophotometrically by following the change in absorbance with time using a UV–visible spectrophotometer for slower reactions or stopped-flow techniques for ultrafast reactions.

Table 2 DFT minimum energy structures and frontier molecular orbitals of the complexes

Optimised structures	HOMO	LUMO
C1		
C2		
C3		
C4		
C5		
C6		

All reactions were thermostated with a precision of $\pm 0.1\ ^\circ$C of the set temperature. The spectral data taken at a wavelength of maximum absorption changes were fitted to a first-order exponential decay function to obtain the observed pseudo-first-order rate constants, k_{obs}, according to Eq. 1 [45].

$$A_t = A_\circ + \left(A_\circ - A_\infty\right)\exp\left(-k_{obs}t\right) \tag{1}$$

where A_0 is initial absorbance of the mixture at time $t = 0$, A_t is absorbance of the reaction mixture at any time, t and A_∞ is final absorbance.

Typical absorbance spectral changes are illustrated in Fig. 4 for the reaction of 0.01 mM C4 with 0.5 mM TU (inset is the respective kinetic trace at 300 nm). Other kinetic traces are placed in the supporting information Fig. ESI 18, 21, 24 and 27.

The average values of observed rate constant were plotted against nucleophile concentrations according to Eq. 1. The tabled data on the values of nucleophile concentration and k_{obs} are presented in supporting information Tables ESI 1, 4, 7, 10, 12 and 14.

$$k_{obs} = k_2[\text{Nu}] + k_{-2} \sim k_2[\text{Nu}] \tag{2}$$

The plots are linear with the slopes representing the second-order rate constants, k_2. Typical plots of k_{obs} verses [Nu] are shown in Fig. 5 for the substitution reactions of C6 with the thiourea nucleophiles at 298 K. More sample plots of observed rate constant, k_{obs}, versus concentration of nucleophile are presented in supporting information Fig. ESI 13, 14, 16, 19, 22, 25 and 28.

Mechanism of substitution

From the kinetic analysis, Scheme 2 illustrates the substitution reactions for the tri-aqua (a) and mono-aqua (b) complexes.

The temperature dependence of the second-order rate constants was studied over the temperature range of 20–40 °C in increments of 5 °C. Data were subjected to a linear plot of $\ln(k_2/T)$ against T^{-1}/K^{-1} (the Eyring plot) according to Eq. 3

$$\ln\left(\frac{k_{exp}}{T}\right) = \frac{-\Delta H^{\neq}}{R}\cdot\frac{1}{T} + \left[23.8 + \frac{\Delta S^{\neq}}{R}\right] \tag{3}$$

Typical Eyring plots are shown in Fig. 6 for the reactions of C4 with the thiourea nucleophiles.

The slopes and intercepts of the Eyring plots gave the enthalpy of activation, $\Delta H^{\neq}$, and entropy of activation, $\Delta S^{\neq}$, values, respectively. Values of the activation parameters are reported in Table 4. The rest of the Eyring plots are placed in supporting information Fig. ESI 15, 17, 20, 23 and 26 and the tables showing values of $\ln(k_2/T)$ and T^{-1}/K^{-1} are found
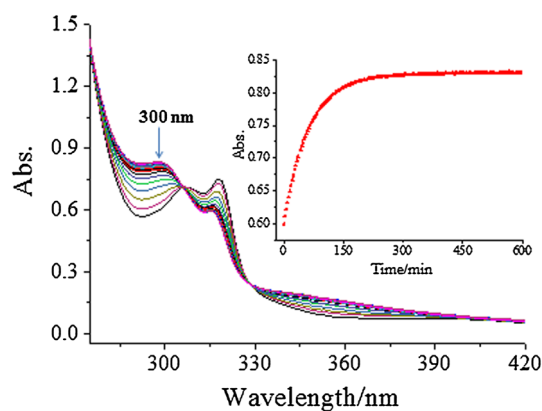

Fig. 4 UV–visible spectra for the reaction of 0.01 mM C4 with 0.5 mM TU at 298 K (inset is a kinetic trace at 300 nm)
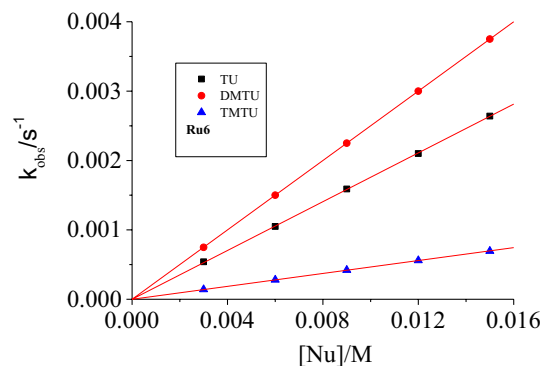

Fig. 5 Plots of k_{obs} versus nucleophile concentration for the reaction of C6 with the thiourea nucleophiles at 298 K

in the supporting information in Tables ESI 3, 6, 9, 11 and 13. The values of k_2, $\Delta H^{\neq}$ and $\Delta S^{\neq}$ are reported in Table 4.

Discussion

The arene-Ru(II) complexes have η^6-arene ligands, whose extended π molecular orbitals (ring MOs) can side overlap with the metal d (σ-/or π-) atomic orbitals, contributing a total of 6π-electrons into the molecular orbitals of the complex. The other coordination sides are occupied by three aqua ligands (C1–2) or an N,N-bidentate ligand and the aqua labile group (C3–6) [54]. Substituents on the η^6-arene ligands affect the electron distribution in the ligand and thus the electron density around the Ru(II) metal centre and its effect on the leaving group. Dadc et al. [55] made a similar point when they observed that alkylated η^6-arene ligands had stronger σ/π-donor character towards the metal centre.

The geometry in most arene complexes is pseudo-octahedral, characterized by the arene and three other groups at the base of a piano stool [9, 28, 55, 56]. The other groups are

Scheme 2 Illustrations of the substitution reactions for complexes under investigation
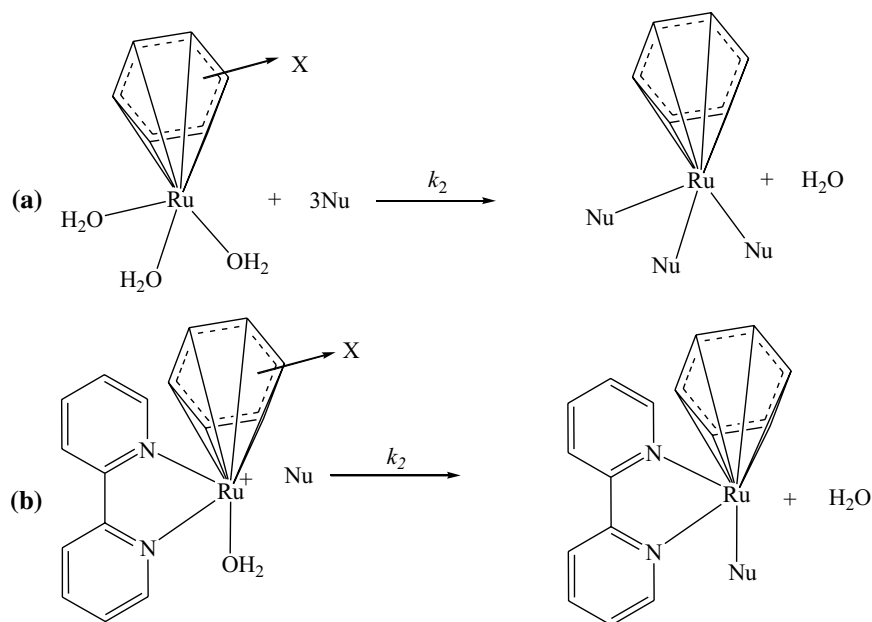
X = (a) benzene (**C1**) or mesitylene (**C2**). (b) benzene (**C3**), mesitylene (**C4**), hexamethylbenzene (**C5**) or *p*-cymene (**C6**). Nu = TU, DMTU or TMTU
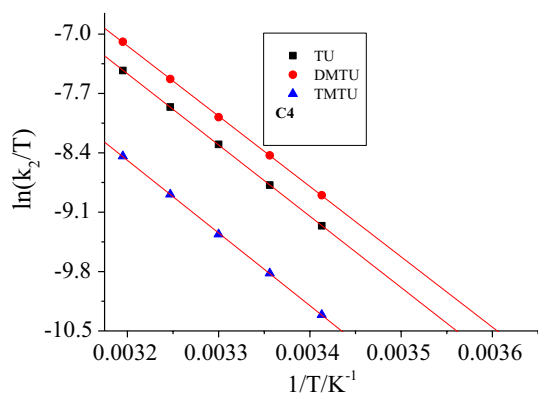

Fig. 6 Eyring plots for the reactions of C4 with thiourea nucleophiles

spatially distributed so as to minimize electron repulsions between bonded and non-bonded electron pairs. However, introduction of the bipyridyl ligand in C1 and C2 further distorts the piano-stool geometry to a near T-geometry for complexes C3–6 orienting the aqua ligand directly trans to the face of the η^6-arene ligand as depicted in Fig. 2. This positions the η^6-arene ligand to have a labializing effect on the aqua leaving group via a ground state destabilizing (the trans influence). This supposition is in line with the DFT-optimized structures of these complexes, and a depiction of this geometry is shown in Fig. 2 for C3. In the optimized structures of C3–6, the angle C8–Ru1–O7 is almost linear (180°) while angle N(2)–Ru(1)–O(7) is 90° (Table 3),

showing the bipyridine ligand is perpendicular to the trans axis.

This geometry is corroborated by X-ray crystal structure literature data of C3 [57]. Data in Table 4 show that the order of reactivity of the complexes is C1 > C2 > C5 > C4 > C6 > C3. C1 is more reactive than C2 because of the inductive donor effect of the three methyl groups on the η^6-mesitylene ligand of C2. As a result, electron density is accumulated at the Ru metal centre of C2 thereby lowering the electrophilicity of the complex. This causes lower rates of substitution from C2. This is supported by the DFT calculated NBO charges showing higher charge for C1 (0.430) compared to C2 (0.377). The electrophilicity index of C1 (6.612) is also higher than that of C2 (4.998) (Table 3). A more positive metal centre pulls the incoming nucleophiles more strongly [58] hence the higher reactivity shown by C1. It is worth noting that the structures of C1 and C2 are trigonal pyramidal in geometry eliminating the possibility of aqua–arene trans orientation. The consequence is that trans effect is minimal or non-existent in these complexes even though electrons are donated towards the ruthenium metal centre.

Other DFT calculated quantities including chemical hardness and electronic chemical potential further support the observed trend in the rate of substitution as envisaged in the literature [16, 59–62]. The HOMO–LUMO energy gap for C1(4.514) is smaller than that of C2 (4.536) which makes it easier for electron density to be transferred from the HOMO to the LUMO increasing the electrophilicity of the Ru(II)

Table 3 Summary of DFT calculated data for the studied complexes

Parameters	C1	C2	C3	C4	C5	C6
Bond lengths (Å)						
Ru(1)–O(7)	2.13	2.15	2.15	2.15	2.17	2.15
Bond angles (°)						
C(8)–Ru(1)–O(7)	100.1	111.1	174.6	173.9	173.0	174.4
N(2)–Ru(1)–O(7)	–	–	85.2	85.8	85.9	84.4
NBO charges						
Ru(1)	0.430	0.377	0.276	0.281	0.314	0.280
O(7)	− 0.710	− 0.874	− 0.859	− 0.860	− 0.869	− 0.862
Orbital energy/eV						
HOMO	− 7.720	− 7.444	− 7.018	− 6.945	− 6.718	− 7.140
LUMO	− 3.206	− 2.908	− 3.057	− 3.007	− 2.951	− 3.070
$\Delta E_{HOMO-LUMO}$	4.514	4.536	3.961	3.938	3.767	4.072
Global chemical reactivity indices						
η/eV	2.257	2.268	1.981	1.969	1.884	2.036
μ/eV	− 5.463	− 5.176	− 5.038	− 4.976	− 4.835	− 5.204
ω/eV	6.612	4.998	6.406	6.288	6.203	6.4000

η, chemical hardness; μ electronic chemical potential; ω, global electrophilicity index

metal centre, thus the higher reactivity of C1. The stability of C1 (2.257) is less than that of C2 (2.268) which confirms the higher reactivity of C1. The electronic chemical potential of C1 (− 5.463) is lower than that of C2 (− 5.176) which indicates a less tendency for electrons to escape from C1 implying it is more positive than C2 hence more reactive.

For the complexes C3–C6 which bear 2,2′-bipyridyl as a common auxiliary ligand, the order of reactivity is C3 < C6 < C4 < C5. The rate of substitution increases with the number of alkyl substituents attached onto the η^6-arene ligand. The number of alkyl substituents attached directly onto the arene in the 2,2′-bypyridyl(η^6-arene)Ru(II) complexes increase in the order 0 (C3) > 2 (C6) > 3 (C4) > 6 (C5). The higher the number of alkyl groups on the η^6-arene ligand, the stronger the inductive donation of electron density into the π-group molecular orbitals of the ring and hence the more electron density flowing into the coordination bonds with Ru. This labializes the aqua groups through the trans influence. This is also raises the HOMO orbitals of the complexes in the same order while the LUMOSs are hardly affected, showing the ground state labialisation effect on the properties of the complexes.
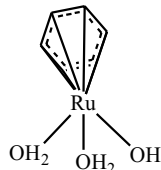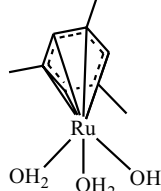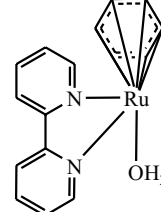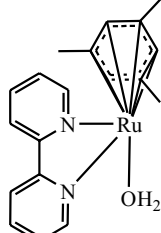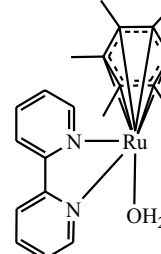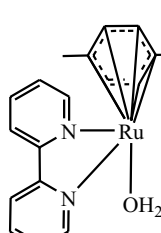
This has been observed in the literature for similar structured complexes exhibiting trans influence [63]. This inductive donation of electron density into the π-group molecular orbitals and towards the Ru centres also causes accumulation of electron density on the Ru metal centre as supported by the decrease in electrophilicity indices, ω, of the 2,2′ bypyridyl(η^6-arene)Ru(II) (6.203 (C5) > 6.288 (C4) > 6.400 (C6) > 6.406 (C3) with increase in the number of alkyl groups on the arene ligands [64]. The rest of DFT calculated data (Table 3) is consistent with the observed kinetic trends as envisioned in the literature [65]. The HOMO–LUMO energy gaps of 2,2′ bypyridyl(η^6-arene)Ru(II) increase in the order 3.767 (C5) < 3.938 (C4) < 4.072 (C6) ∼ 3.961 (C3), signifying a decreased capacity of the arene ligands to receive electron density form the metals by π-back bonding leading to decreased reactivity in that order. The chemical hardness values increase in the same order as the energy gap: [1.884 (C5) < 1.969 (C4) < 2.036 (C6) ∼ 1.981 (C3)]. The electronic chemical potential (eV) values decrease [− 4.835 (C5) > − 4.976 (C4) > − 5.204 (C6) ∼ − 5.038 (C3)] in the same trend as the rate of substitution reactivity.

The (tri-aqua)(η^6-arene)Ru(II) complexes C1 and C2 are approximately 10^2 more reactive than their mono-aqua-Ru(II) counterparts C3 and C4, respectively. This is because the introduction of the bipyridyl ligand introduces steric hindrance at the Ru(II) metal centre which restricts the incoming nucleophiles, this effect has also been reported in the literature [54].

The values of $\Delta S^{\neq}$ are negative while the values of $\Delta H^{\neq}$ are positive and low; hence, the mode of substitution is associative and proceed through a seven-coordinate at the Ru(II) metal centre in the transition state. There is reported literature in support of this mechanism of substitution for octahedral Ru(II) complexes [57]. The thiourea nucleophiles substituted the aqua ligands in the order DMTU > TU > TMTU. The DMTU reacts faster than TU because its two methyl groups donate electron density inductively towards the sulphur atom making it more nucleophilic hence more reactive. This has been reported in the literature for similar studies [66–71]. The nucleophile TMTU could be predicted to be more reactive based on nucleophilicity but is observed to be least reactive because the increased methyl groups attached to the sulphur atom result in higher steric hindrance.

Table 4 Rate constants at 298 K and activation parameters for studied reactions

Complexes		Nu	$k_2/M^{-1}s^{-1}$ x 10^{-1}	$\Delta H_2^{\neq}$ (kJ/mol)	$\Delta S_2^{\neq}$ (J/K/mol)
	C1	TU	118 ± 2	44 ± 1	− 57 ± 3
		DMTU	86 ± 3	56 ± 2	− 20 ± 5
		TMTU	45 ± 4	59 ± 1	− 16 ± 3
	C2	TU	53.8 ± 0.1	68 ± 1	− 41 ± 3
		DMTU	37.2 ± 0.1	68 ± 3	− 18 ± 7
		TMTU	24.8 ± 0.03	75 ± 1	− 10 ± 3
	C3	TU	0.69 ± 0.01	68 ± 1	− 32 ± 3
		DMTU	0.71 ± 0.01	65 ± 2	− 31 ± 5
		TMTU	0.07 ± 0.01	69 ± 1	− 31 ± 3
	C4	TU	0.96 ± 0.01	66 ± 3	− 36 ± 7
		DMTU	1.30 ± 0.01	70 ± 1	− 33 ± 3
		TMTU	0.14 ± 0.01	71 ± 2	− 40 ± 5
	C5	TU	2.26 ± 0.01	60 ± 1	− 56 ± 3
		DMTU	3.22 ± 0.01	58 ± 1	− 59 ± 3
		TMTU	0.94 ± 0.03	65 ± 1	− 47 ± 3
	C6	TU	0.74 ± 0.01	63 ± 1	− 50 ± 3
		DMTU	1.02 ± 0.01	64 ± 3	− 45 ± 8
		TMTU	0.22 ± 0.01	67 ± 1	− 46 ± 3

Conclusions

The reactivity of the Ru(II) complexes is controlled by the nature and type of ligands coordinated to the metal centre. The introduction of the bipyridyl ligand to C1 and C2 to form C3 and C4, respectively, alters their piano-stool geometry to a T-geometry in which the aqua ligand is directly trans to the face of the η^6-arene. The alkylated η^6-arene ligands receive electron density by inductive donation into its extended molecular orbitals which can be π-donated to the Ru metal centre. The higher the number of alkyl groups on the arene ligand, the stronger the inductive

donation. The greater inductive electron donation in C2 makes its metal centre less electropositive than that of C1 hence less reactive. Complexes C3–C6 having 2,2′-bipyridyl ligand reacted in the order C3 < C6 < C4 < C5 in line with an increased labilizing effect on the aqua co-ligand through the trans influence of the alkylated η^6-arene ligands. The bipyridyl ligand also introduces steric hindrance at the Ru metal centre, lowering the reactivity of the complexes C3–C6 compared to C1 and C2. The mode of substitution in these complexes is associative in nature.

Compliance with ethical standards

Conflict of interest The authors declare that they have no conflict of interest as far as this work is concerned.

References

1. Reedijk J (2003) Proc Natl Acad Sci 100:3611
2. Zhao Y, He W, Shi P, Zhu J, Qiu L, Lin L, Guo Z (2006) Dalton Trans 22:2617–2619
3. Novakova O, Chen H, Vrana O, Rodger A, Sadler PJ, Brabec V (2003) Biochemistry 42:11544–11554
4. Montero EI, Pérez JM, Schwartz A, Fuertes MA, Malinge JM, Alonso C, Leng M, Navarro-Ranninger C (2002) ChemBioChem 3:61–67
5. Gallori E, Vettori C, Alessio E, Vilchez FG, Vilaplana R, Orioli P, Casini A, Messori L (2000) Arch Biochem Biophys 376:156–162
6. Singh SK, Joshi S, Singh AR, Saxena JK, Pandey KD (2007) Inorg Chem 46(25):10869–10876
7. Siddik ZH (2003) Oncogene 22:7265–7279
8. Han Ang W, Dyson PJ (2006) Eur J Inorg Chem 2006:4003–4018
9. Wang F, Chen H, Parsons S, Oswald IDH, Davidson JE, Sadler PJ (2003) Chem A Eur J 9:5810–5820
10. Jiang C-W, Chao H, Li H, Ji L-N (2003) J Inorg Biochem 93:247–255
11. Beck JL, Gupta R, Urathamakul T, Williamson NL, Sheil MM, Aldrich-Wright JR, Ralph SF (2003) Chem Commun 5:626–627
12. Ambroise A, Maiya BG (2000) Inorg Chem 39:4264–4272
13. Hartinger CG, Dyson PJ (2009) Chem Soc Rev 38:391–401
14. Groessl M, Hartinger CG, Połeć-Pawlak K, Jarosz M, Dyson PJ, Keppler BK (2008) Chem Biodivers 5:1609–1614
15. Dyson PJ, Sava G (2006) Dalton Trans 16:1929–1933
16. Morris RE, Aird RE, Murdoch Pdel S, Chen H, Cummings J, Hughes ND, Parsons S, Parkin A, Boyd G, Jodrell DI, Sadler PJ (2001) J Med Chem 44:3616–3621
17. Novakova O, Malina J, Suchankova T, Kasparkova J, Bugarcic T, Sadler PJ, Brabec V (2010) Chem A Eur J 16:5744–5754
18. Smalley KSM, Contractor R, Haass NK, Kulp AN, Atilla-Gokcumen GE, Williams DS, Bregman H, Flaherty KT, Soengas MS, Meggers R, Herlyn M (2007) Can Res 67:209–217
19. Magennis WS, Habtemariam A, Novakova O, Henry JB, Meier S, Parsons S, Oswald IDH, Brabec V, Sadler PJ (2007) Inorg Chem 46:5059–5068
20. Scolaro C, Chaplin AB, Hartinger CG, Bergamo A, Cocchietto M, Keppler KB, Sava G, Dyson PJ (2007) Dalton Trans 43:5065–5072
21. Lo KK-W, Lee TK-M (2004) Inorg Chem 43:5275–5282
22. Peacock AF, Habtemariam A, Fernández R, Walland V, Fabbiani FP, Parsons S, Aird RE, Jodrell DI, Sadler PJ (2006) J Am Chem Soc 128:1739–1748
23. Liu Y, Hammitt R, Lutterman DA, Joyce LE, Thummel RP, Turro C (2009) Inorg Chem 48:375–385
24. Chatterjee S, Kundu S, Bhattacharyya A, Hartinger CG, Dyson PJ (2008) J Biol Inorg Chem 13:1149–1155
25. Aird RE, Cummings J, Ritchie AA, Muir M, Morris RE, Chen H, Sadler PJ, Jodrell DI (2002) Br J Cancer 86:1652–1657
26. Novakova O, Kasparkova J, Bursova V, Hofr C, Vojtiskova M, Chen H, Sadler PJ, Brabec V (2005) Chem Biol 12:121–129
27. Liu HK, Sadler PJ (2011) Acc Chem Res 44:349–359
28. Kumar P, Gupta RK, Pandey DS (2014) Chem Soc Rev 43:707–733
29. Ang WH, Daldini E, Scolaro C, Scopelliti R, Juillerat-Jeannerat L, Dyson PJ (2006) Inorg Chem 45:9006–9013
30. Wesselinova D, Kaloyanov N, Dimitrov G (2009) J Med Chem 44:5099–5102
31. Bruijnincx PC, Sadler PJ (2008) Curr Opin Chem Biol 12:197–206
32. Dayan O, Dayan S, Kani I, Çetinkaya B (2012) Appl Organomet Chem 26:663–670
33. Enos G, Mambanda A, Jaganyi D (2013) J Coord Chem 66:4280–4291
34. Bugarčić ŽD, Petrović BV, Jelić R (2001) Transition Met Chem 26:668–671
35. Hochreuther S, Puchta R, van Eldik R (2011) Inorg Chem 50:8984–8996
36. Jaganyi D, Tiba F, Munro OQ, Petrović B, Bugarčić ŽD (2006) Dalton Trans 24:2943–2949
37. Mambanda A, Jaganyi D (2011) Dalton Trans 40:79–91
38. Gaussian RA (2009) Inc., Wallingford CT 121:150–166
39. Hay PJ, Wadt WR (1985) J Chem Phys 82:270–283
40. Lee C, Yang W, Parr RG (1988) Phys Rev B 37:785
41. Becke AD (1993) J Chem Phys 98:5648–5652
42. Okamura M, Yoshida M, Kuga R, Sakai K, Kondo M, Masaoka S (2012) Dalton Trans 41:13081–13089
43. Cossi M, Rega N, Scalmani G, Barone V (2003) J Comput Chem 24:669–681
44. Le Bahers T, Pauporté T, Scalmani G, Adamo C, Ciofini I (2009) Phys Chem Chem Phys 11:11276–11284
45. Shaira A, Jaganyi D (2014) J Coord Chem 67:2843–2857
46. Chattaraj PK, Sarkar U, Elango M, Parthasarathi R, Subramanian V (2005) arXiv preprint physics/0509089
47. Cedillo A, Contreras R (2012) J Mex Chem Soc 56(3):257–260
48. Weinhold F, Landis CR, Glendening ED (2016) Int Rev Phys Chem 35(3):399–440
49. Parr RG, Yang W (1989) J Chem Phys 98:5648
50. Geerlings P, De Proft F, Langenaeker W (2003) Chem Rev 103:1793–1874
51. Parr RG, Yang W (1984) J Am Chem Soc 106:4049–4050
52. Yang W, Mortier WJ (1986) J Am Chem Soc 108:5708–5711
53. Sangilipandi S, Sutradhar D, Bhattacharjee K, Kaminsky W, Joshi SR, Chandra AK, Rao KM (2016) Inorg Chim Acta 441:95–108
54. Warren SG, Clayden J (2001) Solutions manual to accompany organic chemistry by Clayden, Greeves, Warren, and Wothers. Oxford University Press, Oxford

55. Dadci L, Elias H, Frey U, Hoernig A, Koelle U, Merbach AE, Paulus H, Schneider JS (1995) Inorg Chem 34:306–315
56. Tripathy SK, De U, Dehury N, Pal S, Kim HS, Patra S (2014) Dalton Trans 43:14546–14549
57. Tiba F, Jaganyi D, Mambanda A (2010) J Coord Chem 63:2542–2560
58. Wekesa IM, Jaganyi D (2014) Dalton Trans 43:2549–2558
59. Mebi CA (2011) J Chem Sci 123:727–731
60. Vektariene A, Vektaris G, Svoboda J (2009) ARKIVOC Online J Organ Chem 7:311–329
61. Parr RG, Pearson RG (1983) J Am Chem Soc 105:7512–7516
62. Liu S (2005) J Chem Sci 117:477–483
63. Coe BJ, Glenwright SJ (2000) Coord Chem Rev 203:5–80
64. Parr RG, Szentpaly LV, Liu S (1999) J Am Chem Soc 121:1922–1924
65. Jaganyi D, Sitati MK, Wekesa IM (2016) Inorg Chim Acta 453:531–537
66. Asman WP, Jaganyi D (2017) Int J Chem Kinet 49:545–561
67. Petrović B, Bugarčić ZID, Dees A, Ivanović-Burmazović I, Heinemann FW, Puchta R, Steinmann SN, Corminboeuf C, Van Eldik R (2012) Inorg Chem 51:1516–1529
68. Milutinović MM, Elmroth SKC, Davidović G, Rilak A, Klisurić OR, Bratsos I, Bugarčić ŽD (2017) Dalton Trans 46:2360–2369
69. Rilak A, Bratsos I, Zangrando E, Kljun J, Turel I, Bugarčić ŽD, Alessio E (2014) Inorg Chem 53:6113–6126
70. Milutinović MM, Rilak A, Bratsos I, Klisurić O, Vraneš M, Gligorijević N, Radulović S, Bugarčić ŽD (2017) J Inorg Biochem 169:1–12
71. Chrzanowska M, Katafias A, Impert O, Kozakiewicz A, Surdykowski A, Brzozowska P, Franke A, Zahl A, Puchta R, van Eldik R (2017) Dalton Trans 46:10264–10280